

**DEVELOPMENT OF SURFACE WAVE DISPERSION AND ATTENUATION MAPS AND IMPROVED METHODS FOR MEASURING SURFACE WAVES**

Jeffrey L. Stevens, Jeffrey W. Given, Heming Xu, and G. Eli Baker

Science Applications International Corporation

Sponsored by Air Force Research Laboratory

Contract No. FA8718-05-C-0023

**ABSTRACT**

The objective of this project is to optimize the measurement of surface waves, particularly at regional and local distances and at periods of 8–15 seconds. One goal of this project is the development of global regionalized dispersion and attenuation maps, with a particular focus on determining attenuation maps for Eurasia in the 8–15 second period band. Both the dispersion and attenuation maps are corrected for scattering and diffraction from heterogeneous earth structure. Successful application of these corrections requires an understanding of the characteristics of surface wave propagation in regions of variability high enough that common correction methods may fail. We implemented the algorithm of Zhou et al. (2004) for calculating finite frequency sensitivity kernels for dispersion and amplitude variations, and have been testing the algorithms using the one-degree dispersion maps of Stevens et al. (2005). Amplitude corrections predicted by the Born approximation are unreasonably large for long paths. In order to determine under what conditions the Born approximation gives valid results, we performed a 3D finite difference calculation using an earth model for the Tarim Basin embedded in a uniform structure typical of the Eurasian shield regions, and then compared the results with variations predicted by the Born approximation. The predicted wavefields were compared out to a distance of several hundred km. The Born approximation is generally consistent with the finite-difference results, but there are localized, strong interference effects in the finite-difference results not apparent in the Born calculation. The approximation is less accurate at a 10-s period than at a 20-s period.

We are also developing a “path corrected surface wave magnitude,” which combines the time domain narrow-band surface wave magnitude procedure of Russell (2006) with the path corrected spectral magnitude of Stevens and McLaughlin (2001). This allows the magnitude to be regionalized to account for variations in amplitude due to differences in earth structure and attenuation. We perform a detailed comparison of these magnitude types and then apply them to data from the North Korean nuclear test. We calculate frequency dependent amplitude corrections using the Born approximation for surface waves along paths that recorded the North Korean explosion. The path corrected spectra for these data are flat to the north and south, and much more frequency dependent and larger in amplitude at stations to the west. The Born corrections are also flat to the north and south and much more variable along the other paths; however, they do not match the observations very well. This is probably either because the resolution of the models is insufficient or because the variability exceeds the limits of the Born approximation. The amplitude variations are too large to be explained by attenuation differences on these short paths, and they are also too large to be explained by tectonic release given the lack of observed Love waves, so structural effects are the most likely cause of the variations.

We are in the process of analyzing data for a large Eurasian data set and are attempting to separate amplitude variations due to attenuation from amplitude variations due to structure. We have collected data from Eurasian explosions at the Lop Nor and Balapan test sites, and from more recent earthquakes recorded at a high station density within the Eurasian continent. We are measuring amplitude variations, and then identifying the components of the amplitude variation, which are: 1) radiation pattern; 2) attenuation; 3) variations due to path structure; 4) variations due to off-path structure; and 5) unmodeled variations. After the analysis is completed, this attenuation data set will be used to invert for Q structure, which will then be used to generate maps that predict surface wave amplitudes due to earth structure and attenuation.

**OBJECTIVES**

The objective of this project is to optimize the measurement of surface waves, particularly at regional and local distances and at periods of 8–15 seconds. One goal of the project is the development of global regionalized dispersion and attenuation maps, with a particular focus on determining attenuation maps for Eurasia in the 8–15 second period band. Both the dispersion and attenuation maps are being corrected for scattering and diffraction from heterogeneous earth structure. We also implement a path corrected surface wave magnitude, which combines the time domain narrow-band surface wave magnitude procedure of Russell (2006) with the path corrected spectral magnitude of Stevens and McLaughlin (2001).

**RESEARCH ACCOMPLISHED**

**Overview**

Surface wave amplitudes are affected by both attenuation and earth structure. The effect on surface wave amplitudes of propagation normal to variations in earth structure is predicted fairly well by conservation of energy. Propagation along paths at grazing incidence to large structure variations, however, are much more difficult to predict. Our main interest in this project is on understanding amplitude variations in 8–15 second surface waves. In this frequency band, surface waves may be affected as strongly or more strongly by earth structure than by intrinsic attenuation, particularly along shorter paths. Our goal is therefore to be able to model and correct for both of these effects. Our approach is illustrated in Figure 1.

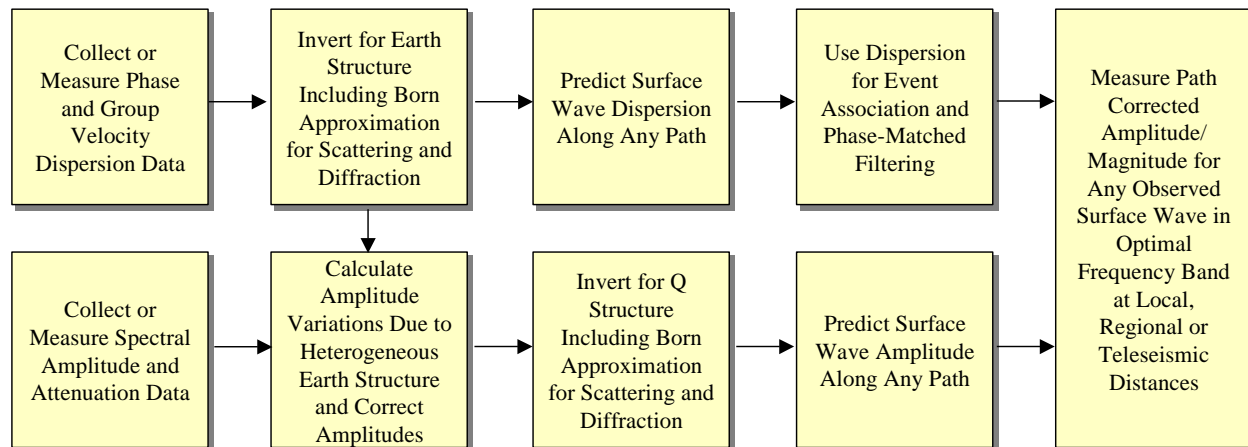


**Figure 1. Overview of the surface wave dispersion and attenuation project.**

In an earlier project (Stevens et al., 2005) we developed global, regionalized dispersion models that allow the phase and group velocity to be calculated between any two points on the earth. We did this by accumulating a large data set consisting of more than 1 million dispersion measurements derived by a number of researchers, and then inverting this data set to determine earth structure, which in turn was used to generate dispersion maps at all frequencies. In that project, we modeled surface waves in a heterogeneous earth using the following approximations: 1) surface waves propagate along great circle paths, 2) surface wave phase and group velocities and anelastic attenuation can be modeled using a path integral between source and receiver, and 3) energy is conserved with no mode conversion across material boundaries. This approximation is quite good for large parts of the world, particularly at lower frequencies, but the unmodeled variations become important in regions of structural complexity.

Separating amplitude variations due to attenuation from amplitude variations due to structure is difficult, so we have been performing experiments using events with well-constrained source mechanisms, using explosions from known test sites and Eurasian earthquakes with centroid moment tensor (CMT) solutions, and looking at pure continental paths. Since we have reasonably good earth models for these paths, we can predict the amplitudes along each path for each event, and then examine the differences between predictions and observations. Because of the large increase in the number of stations over the past couple of decades, there is now a great deal of redundancy for each event, so we can remove the source and predictable path effects with some confidence.

Surface wave magnitudes play an important role in earthquake/explosion discrimination. Three main problems exist with traditional surface wave magnitudes: 1) surface wave dispersion causes amplitude variations unrelated to the source; 2) it is not possible to reliably measure a traditional 20 second surface wave magnitude at local and regional distances because the surface wave is not dispersed enough; and 3) differences in earth structure and attenuation cause variations in surface wave amplitudes that are unrelated to the source. Several surface wave magnitude measurements have been proposed to address these limitations, and we propose some further improvements in the form of a regionalized path corrected surface wave magnitude. In the following section we compare these magnitude types in detail, and then apply them to the North Korean nuclear test. We also use this as an example of separating the surface waves into their component source, receiver and path parts, and examine the residual to show the effect of structural variations.

### Comparison of Butterworth Filtered and Regionalized Surface Wave Magnitudes

Russell (2006) proposed a new type of surface wave magnitude  $M_{s(b)}$  that uses a Butterworth filter to measure a time domain amplitude in a narrow band around any desired frequency, and then applies a correction for the frequency dependence of an explosion source function. The main purpose of  $M_{s(b)}$  is to allow surface waves to be measured at regional distances at higher frequencies than traditional 20 second  $M_s$ . The magnitude is defined by

$$M_{s(b)} = \log A_b + \frac{1}{2} \log \sin \Delta + 0.0031 \left( \frac{20}{T} \right)^{1.8} \Delta - 0.66 \log \left( \frac{20}{T} \right) - \log f_c - 0.43 \quad (1)$$

where  $A_b$  is the filtered amplitude,  $T$  is the measured period, and  $f_c$  is the Butterworth filter width. This magnitude

also requires that the frequency band be less than a minimum value defined by  $f_c \leq \frac{G_{\min}}{T\sqrt{\Delta}}$ . Russell (2006) finds

$G_{\min}=0.6$  for continental structures between 8 and 40 seconds, with smaller values required for deep sediment

structures. Russell (2006) also shows that  $A_b = \frac{f_c T \sqrt{\Delta}}{G} A$  where  $G$  is a constant which for typical continental paths

is approximately 0.93, and  $A$  is the equivalent time domain amplitude. Note that if  $G_{\min}$  is fixed, then the filter

correction corresponds to a distance correction for a normally dispersed (non-Airy phase) surface wave of  $\frac{1}{2} \log \Delta$ .

Stevens and McLaughlin (2001) defined a path corrected spectral magnitude, which similarly was intended to allow surface waves to be measured at all distances and frequencies, and in addition is regionalizeable since it is derived from earth models. The path corrected spectral magnitude,  $\log M_0'$ , is calculated by dividing the observed surface wave spectrum by the Green's function for an explosion of unit moment and taking the logarithm of this ratio, averaged over any desired frequency band. The path corrected spectral magnitude is defined as the logarithm of:

$$M_0' = \left| U_z(\omega, r, \theta) / \left( \frac{S_1^x(\omega, h_x) S_2(\omega) \exp[-\gamma_p(\omega)r]}{\sqrt{a_e} \sin(r/a_e)} \right) \right| \quad (2)$$

where  $U_z$  is the observed vertical component surface wave spectrum,  $S_1^x$  depends on the source region elastic structure and the explosion source depth,  $S_2$  depends on the receiver region elastic structure, and  $\gamma_p$  is the attenuation coefficient that depends on the attenuation integrated over the path between the source and receiver. All of the functions in equation 2 can be derived from plane-layered earth models (see Stevens and McLaughlin, 2001), and allow the measurement to be regionalized to account for differences in earth structure at the source and receiver, and due to attenuation along the path. Since  $M_0'$  is a physical quantity, equation 2 is assumed to be in SI units and  $\log M_0'$  is in  $\log(\text{nt-m})$ ; however, in the following comparison we express  $U_z$  in  $\text{nm-s}$  for consistency with the other amplitude measurements. This adds a constant value of -9 to the normalization constant for  $\log M_0'$ .

Since equations 1 and 2 are both intended to flatten the surface wave spectrum, in principle they can be measured over any desired frequency band. In practice, the path corrected spectral magnitude (equation 2) has been calculated by averaging over a frequency band designed to avoid noise contamination, and has implemented an outlier rejection scheme to minimize bias from spectral dips and noise (Stevens et al., 2005). The implementation of the Butterworth

filtered magnitude (equation 1) by Bonner et al. (2006) has instead used the maximum value over a period band of 8–25 seconds, defined as  $M_s(\text{VMAX})$ , with analyst rejection of outliers.

A path corrected time domain magnitude can be derived by combining the path corrected spectral magnitude with  $M_{s(b)}$ , using the source and path corrections from earth models to replace the empirical corrections. We define the path corrected time domain magnitude  $M_{s(bp)}$  as:

$$M_{s(bp)} = \log A_b + \frac{1}{2} \log \sin \Delta + \gamma_p \Delta \log e - \log S_1 - \log S_2 - \log f_c + C_{bp} \quad (3)$$

where  $C_{bp}$  is a constant chosen to make  $M_{s(bp)}$  consistent with historical magnitudes. By defining  $M_{s(bp)}$  to be equal to Rezapour and Pearce (1998)  $M_s$  at  $50^\circ$ , and simultaneously using the Rezapour and Pearce attenuation rate, and using the mean 20 second value of  $S_1$  and  $S_2$  for Central Asian continental structures ( $\log(S_1)+\log(S_2)=-17.41$ ), we find  $C_{bp}=-17.96$ . We can also define a spectral magnitude directly from equation 2, using the relation (again from

Russell, 2006)  $A_b = \frac{4\pi}{3} f_c U_z$ . This gives  $\log M_0' - M_{s(bp)} = 11.74$ , which is identical to the mean difference

between  $\log M_0'$  and Rezapour and Pearce  $M_s$  found through measurement of a large data set by Stevens and McLaughlin (2001). We can therefore define an equivalent spectral  $M_s$ , which we define as  $M_{s(sp)} = \log M_0' - 11.74$ , which by adding the  $\log M_0'$  normalization constant  $\frac{1}{2} \log(a_e) - 9$  gives an  $M_{s(sp)}$  normalization constant of -17.34. Table 1 shows a comparison of the terms in each of these magnitudes, and in the Rezapour and Pearce  $M_s$ .

**Table 1. Comparison of time domain and spectral magnitude measurement and correction terms**

Magnitude Type	Amplitude Measure	Source	Receiver	Geometric Spreading	Attenuation	Dispersion	Filter	Norm
$M_s$	$\log(A/T)$			$\frac{1}{2} \log \sin \Delta$	$0.0046\Delta$	$\frac{1}{3} \log \Delta$		2.37
$M_{s(b)}$	$\log(A_b)$	$-0.66 \log \left( \frac{20}{T} \right)$		$\frac{1}{2} \log \sin \Delta$	$.0031 \left( \frac{20}{T} \right)^{1.8} \Delta$		$-\log f_c$	-0.43
$\log M_0'$	$\log(U_z)$	$-\log(S_1)$	$-\log(S_2)$	$\frac{1}{2} \log \sin \Delta$	$\gamma_p \Delta \log e$			$\frac{1}{2} \log a_e - 9$
$M_{s(sp)}$	$\log(U_z)$	$-\log(S_1)$	$-\log(S_2)$	$\frac{1}{2} \log \sin \Delta$	$\gamma_p \Delta \log e$			-17.34
$M_{s(bp)}$	$\log(A_b)$	$-\log(S_1)$	$-\log(S_2)$	$\frac{1}{2} \log \sin \Delta$	$\gamma_p \Delta \log e$		$-\log f_c$	-17.96

In this table  $A$  is the traditional time domain 20 second amplitude in nm,  $A_b$  is the Butterworth filtered magnitude (using a 3 pole two pass phaseless filter) in nm, and  $U_z$  is the Fourier spectral amplitude in nm-s. Figure 2 (left) shows a comparison of Russell’s approximation to the explosion excitation function with  $\log(S_1)+\log(S_2)$  (plus a constant to normalize to zero at 20 seconds). As the figure shows, this is a good approximation to the average excitation function across the frequency band; however, there is substantial regional variation in the function that is accounted for in the path corrected magnitudes.

Figure 2 (right) shows that attenuation calculated from earth models is somewhat higher than the Rezapour and Pearce attenuation, and both are higher than the Russell attenuation, which is based on the earlier model of von Seggern (1977). The model-based attenuation corresponds to a Rayleigh wave  $Q$  of about 400, while the Rezapour/Pearce and von Seggern/Russell attenuation correspond to Rayleigh wave  $Q$  of about 550 and 800, respectively. The  $Q$  models are still relatively generic, and are being improved as part of a task in this project; however, the  $Q$  value of 400 is more consistent with empirical Rayleigh wave  $Q$  studies than the higher values of the other magnitudes. This may be because those magnitudes were based on Rayleigh wave amplitudes covering a large distance range, and Rayleigh waves along lower  $Q$  paths may have attenuated away at the larger distances, biasing the attenuation estimates to higher  $Q$  values.

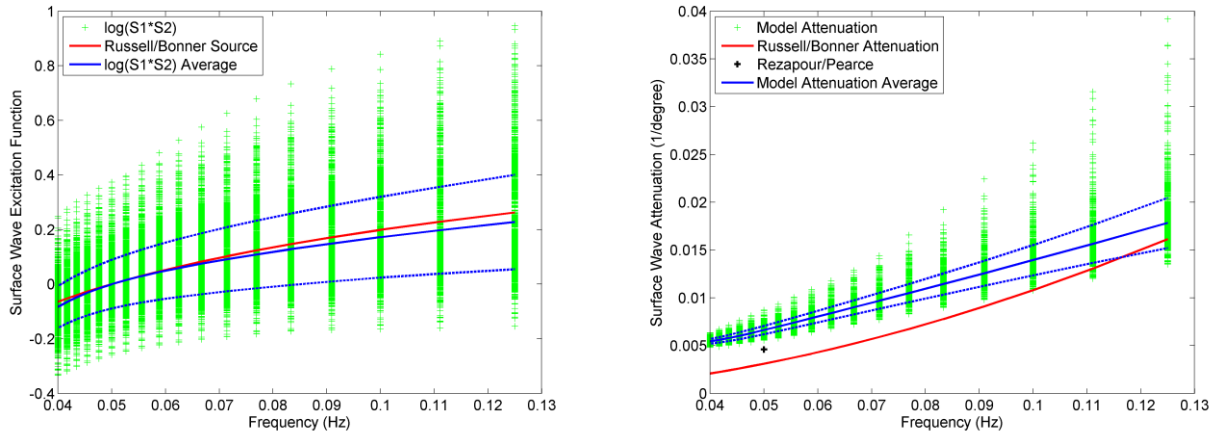


Figure 2. Left: Mean  $\log(S1*S2)$  and  $\pm 1$  standard deviation (blue). Red line shows the Russell approximation for the source function. Right: Mean attenuation and  $\pm 1$  standard deviation (blue) derived from earth models, Russell approximation for attenuation (red), and Rezapour and Pearce global estimate at 20 seconds (black). In both, green marks show values for individual Eurasian structures.

Figure 3 compares the magnitude distance corrections, which are the equations listed in Table 1 calculated with

$$A=1, G_{\min}=0.6, f_c = \frac{G_{\min}}{T\sqrt{\Delta}} \text{ and } A_b = \frac{f_c T \sqrt{\Delta}}{G} A, \text{ for periods of 20 and 10 seconds, respectively.}$$

Differences between the distance corrections are generally small. The main differences are the larger correction at close distances for the Rezapour and Pearce magnitude, and the larger correction for the path corrected magnitude with model-based attenuation at large distances.  $M_{s(bp)}$  will, of course, vary for each source and receiver location corresponding to the particular earth structure and path attenuation. The magnitude correction at close distances is also larger for  $M_{s(b)}$  than for  $M_{s(bp)}$  because the difference in attenuation causes a small difference in the normalization constant which is calculated at 50 degrees.

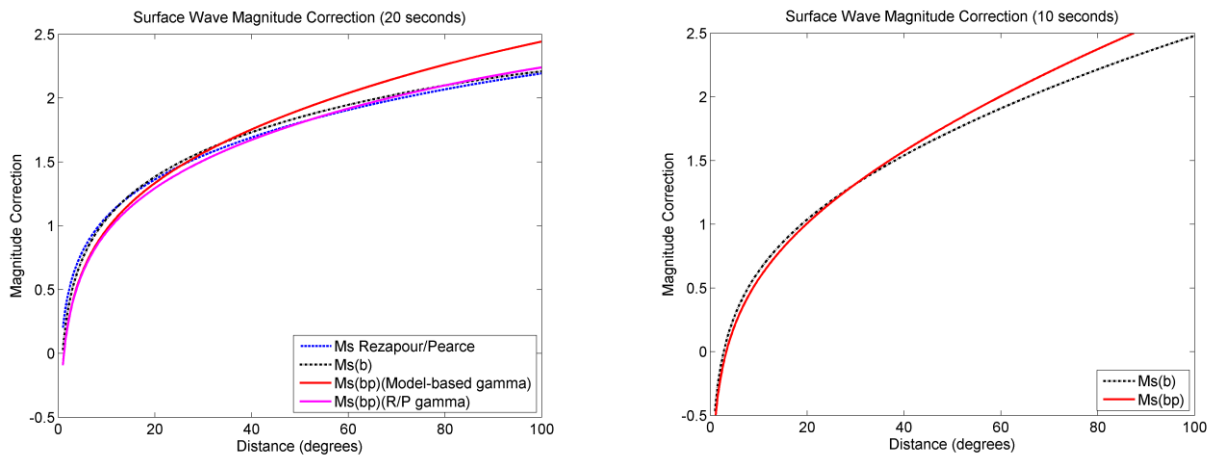


Figure 3. Twenty-second magnitude correction vs distance for Rezapour/Pearce (dashed blue),  $M_{s(b)}$  (dot-dash black),  $M_{s(bp)}$  with model-based gamma (solid red), and  $M_{s(bp)}$  with Rezapour and Pearce gamma (solid maroon) (left). 10 second magnitude correction vs distance  $M_{s(b)}$  (dot-dash black), and  $M_{s(bp)}$  with model-based gamma (solid red) (right).

Analysis of Surface Waves from the North Korean Nuclear Test

To examine the differences between magnitudes in more detail and illustrate some potential problems, we apply the magnitude methods to surface waves from the North Korean nuclear test of October 9, 2006. This is a good test case because the surface waves are small—above noise level at only 7 of the closest stations (Figure 4), difficult to see at all in the unfiltered records, but visible at these stations when low pass filtered (Figure 5).

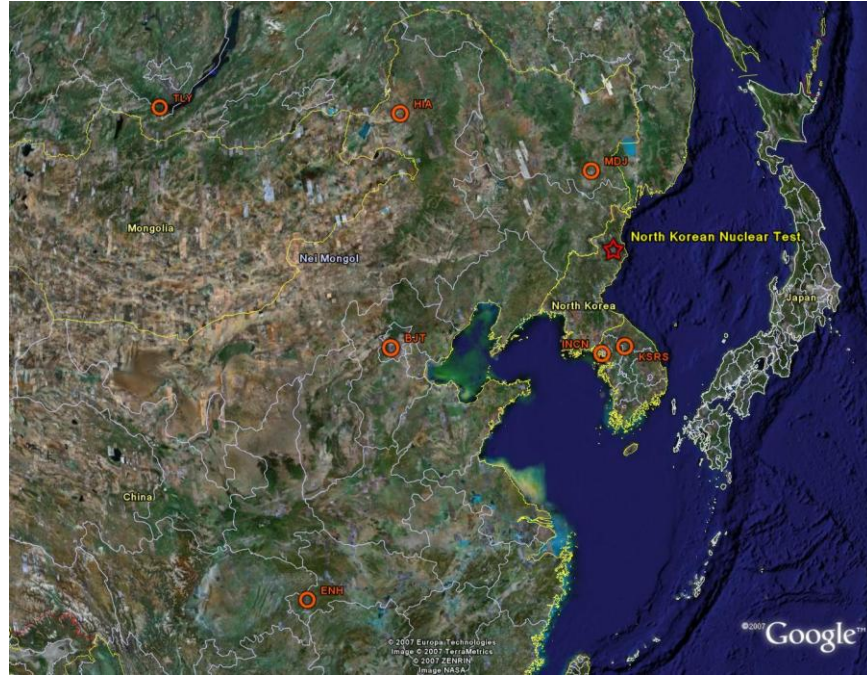


Figure 4. Location of the North Korean nuclear test and recording stations.

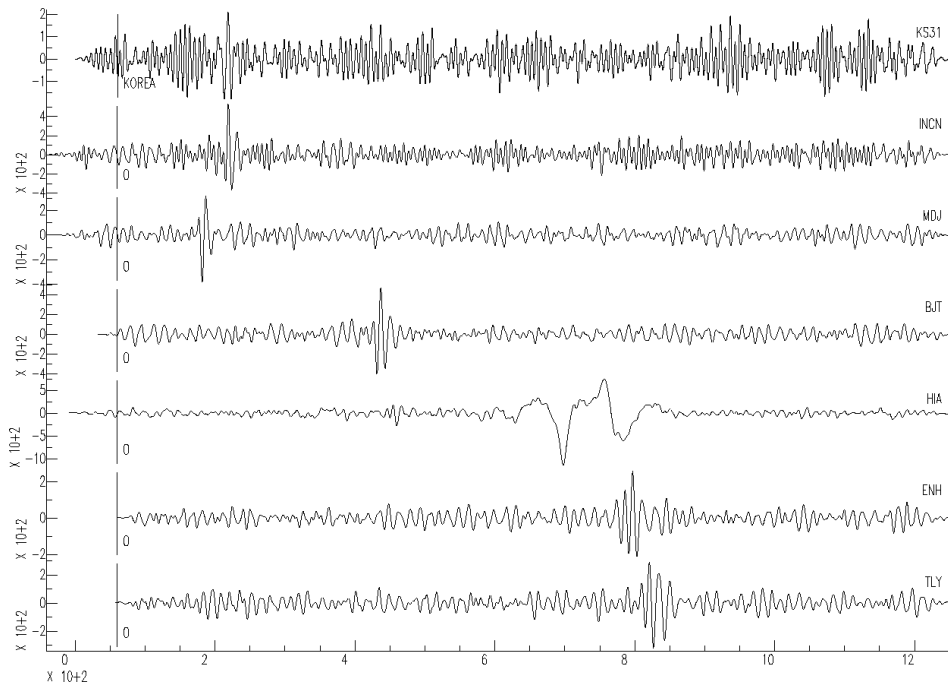
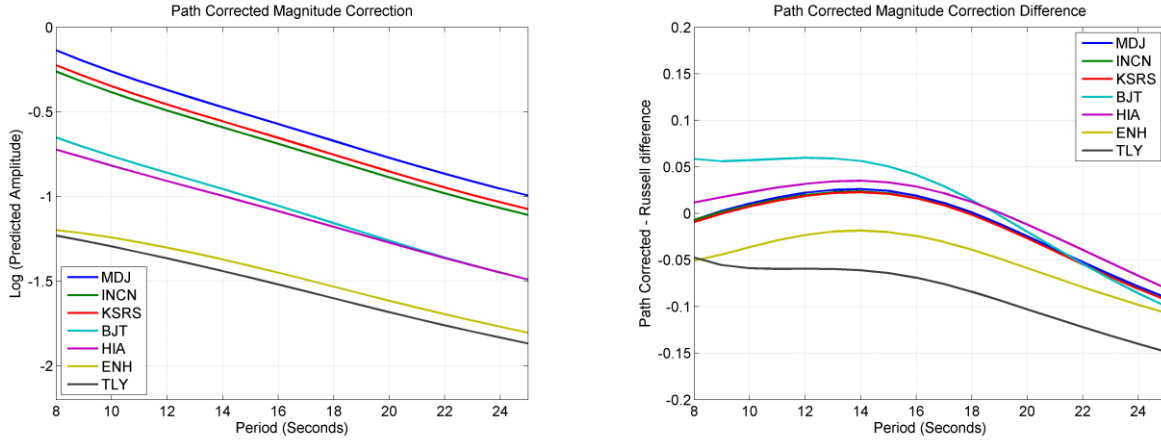


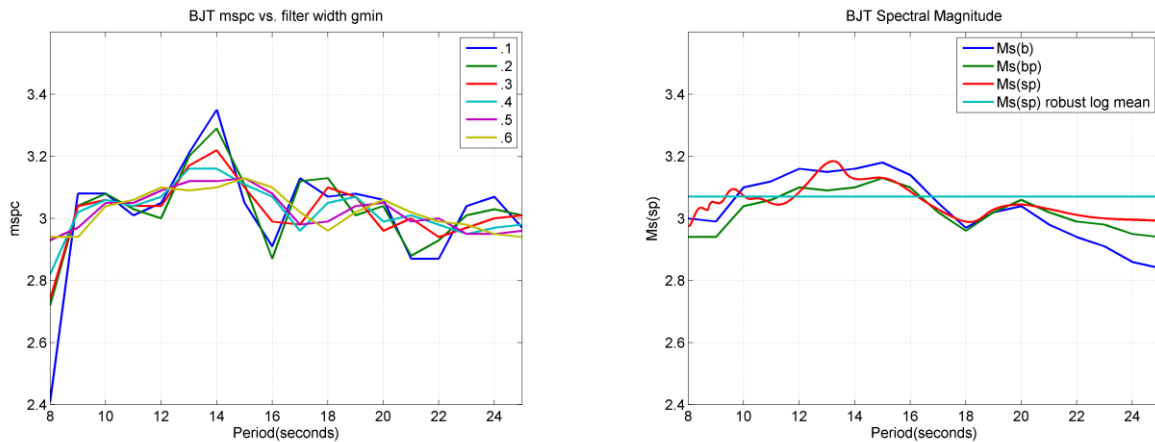
Figure 5. Data from the North Korean explosion filtered from 0.01–0.1 Hz. Surface waves are clearly visible at all stations. HIA has a glitch or interfering arrival after the explosion arrival. The explosion arrival is visible just after the BJT arrival.

Figure 6 shows the predicted spectra at each of the 7 stations based on the model based source and path corrections—these are the negative of the sum of corrections in row 5 of Table 1, and are equivalent to predicted, normalized explosion-generated surface wave spectra at each location. Differences between the model-based and Russell sets of corrections (Figure 6, right) range from -0.15 to 0.05 magnitude units.



**Figure 6. Path corrections for the 7 stations that recorded surface waves from the North Korean nuclear test using model based corrections (left) and differences between the model-based and Russell path corrections for the 7 stations recording the North Korean event.**

Figure 7 (left) shows the calculated Butterworth filtered and path corrected spectral magnitudes for station BJT for 6 values of filter width, as specified by  $G_{min}$  ranging from 0.1 to 0.6. The higher values correspond to wider filter widths which have the effect of smoothing the spectrum and giving more consistent values between frequencies. A disadvantage of the larger values, however, is that the frequency band extends farther outside of the band of interest, possibly allowing contamination by noise or other phases. Figure 7 (right) shows the Butterworth filtered magnitude, the path corrected magnitude, the path corrected spectral magnitude, and the best value of the path corrected spectral magnitude calculated using a robust mean (Stevens et al., 2005). Figure 8 shows a comparison of Butterworth filtered magnitudes with and without path corrections. If the procedure were working perfectly and the surface wave spectra were just like synthetics, then all of the curves in Figures 7 and 8 would be flat lines. The path corrected spectra are slightly flatter than the Butterworth filtered spectra, but it is clear that unmodeled variations are significantly larger than the differences between the individual magnitude curves.



**Figure 7. Calculation of path-corrected Butterworth filtered magnitude for 6 filter widths (left) at station BJT. Butterworth filtered, path corrected, and spectral magnitudes at BJT (right).**

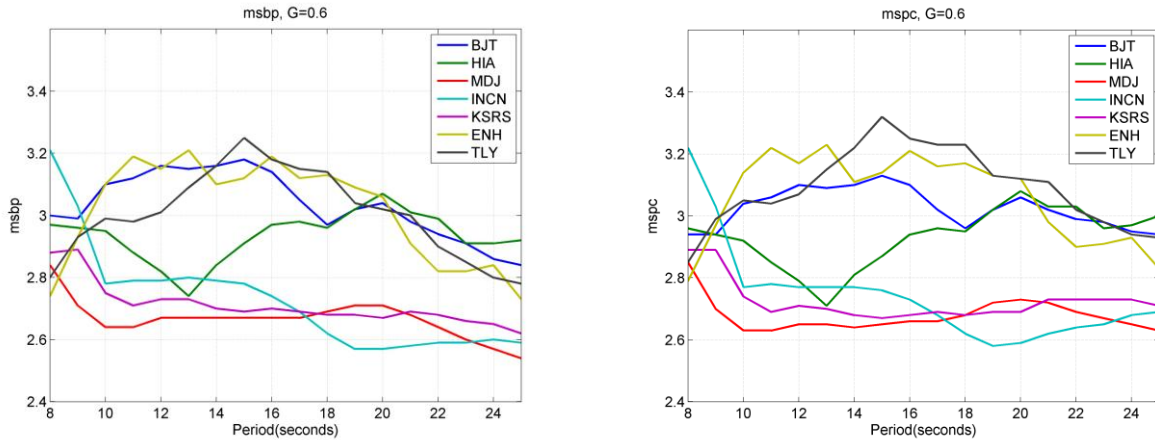


**Figure 8. Butterworth filtered (left) and path corrected (right) magnitudes for the North Korean nuclear test with varying filter widths.**

The spectra divide into two distinct groups—lower values at INCN, KSRS, and MDJ, and higher values at BJT, ENH, and TLY. Station HIA is more complicated, but generally higher. Furthermore, the three lower amplitude stations, which are also the closest stations, have much flatter corrected spectra than the three higher amplitude stations, suggesting a possible frequency dependent amplification of these surface waves. Also, the lower amplitude stations are located due north and south of the event, while the other stations are located to the west (and northwest/southwest) Since we have corrected for source and receiver structure, and attenuation differences could not be responsible for differences this large on paths this short, there are two remaining likely causes for the amplitude variations: tectonic release (or other azimuth dependent source components), and focusing due to path structure.

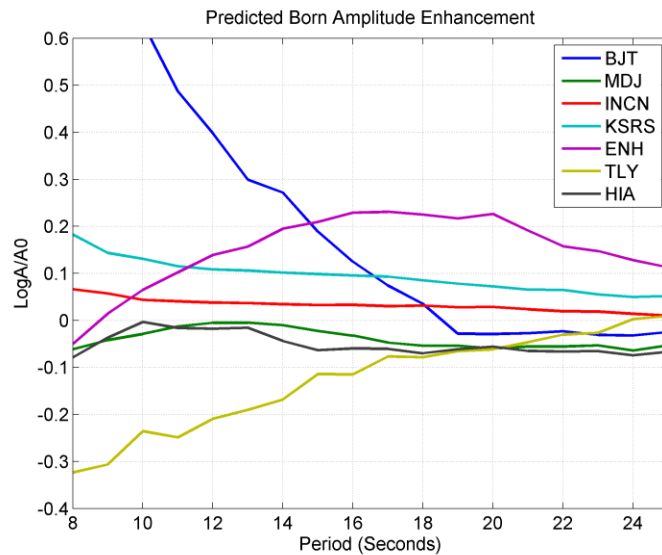


**Figure 9. Amplitude corrections due to structure predicted using the Born approximation.**

The effect of path structure calculated using the Born approximation (Zhou et al., 2004) and the earth models of Stevens et al. (2005) is shown in Figure 9. Although there are clearly some big differences between the predictions and observations, there are also some interesting similarities. First, the corrections for the three closest stations are almost flat and separated by approximately the same amount as the observations. Second, the amplitude correction for ENH is similar to what is observed for ENH and also similar to the observations at TLY and BJT. That is, the data show a peak in the spectrum in the middle periods, dropping back close to the level of the closer stations at the longest and shortest periods. On the other hand a very large amplification, which is not observed, is predicted for

BJT due to a grazing path along the north end of the Yellow Sea, and a big decrease, also not observed, is predicted for TLY. There are two likely explanations for this: 1) the one degree structural resolution is not sufficient for these short paths; and/or 2) the structural complexity exceeds the limits of the Born approximation. The amplification predicted for BJT by the Born approximation, for example, is very strongly dependent on exactly where the station is with respect to the low velocity zone. Also, the Born approximation is known to overpredict amplification at higher frequencies in such cases. Figure 10 shows a comparison of predictions from the Born approximation and a finite difference calculation for waves propagating near the Tarim Basin, another low velocity zone. The red band to the upper left of the Tarim Basin is the same amplification effect that is occurring in Figure 9 for station BJT. As shown in the finite difference calculation figure, this type of amplification stretches the limits of the Born approximation, and the actual amplification is smaller and more complicated. The comparison between the Born approximation and finite difference is much better at 20 seconds (see Stevens et al., 2006), so it is possible that in regions of structural complexity the Born approximation is adequate at 20 seconds but inadequate at 10 seconds.

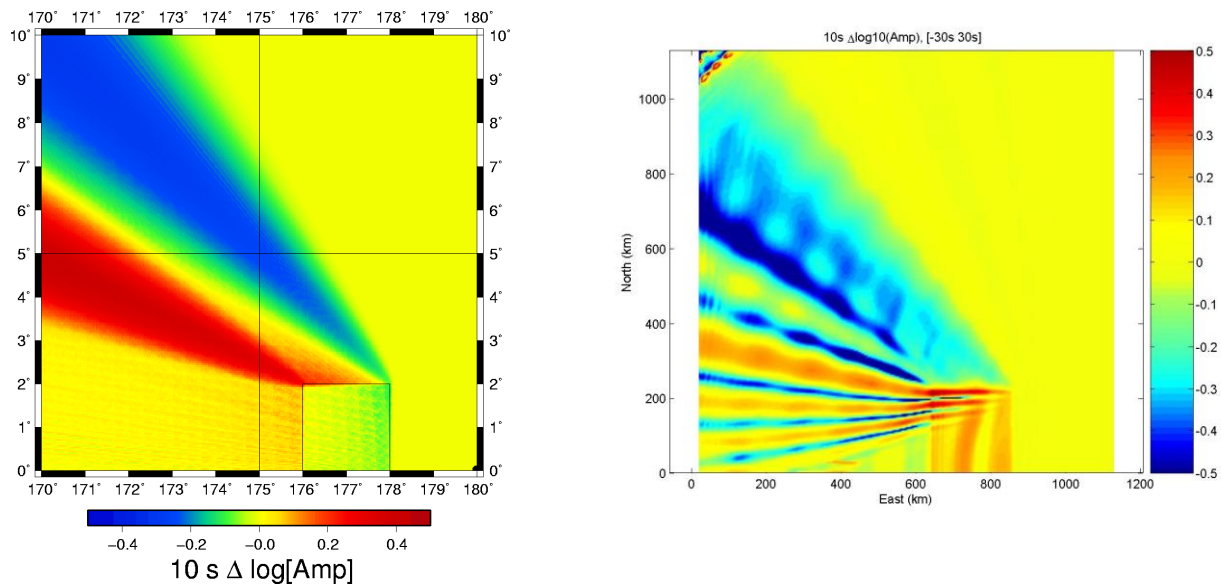


**Figure 10. Comparison of Born approximation (left) with finite difference calculation (right) of amplitude perturbations at 10 seconds. The rectangular inclusion is modeled after the Tarim Basin structure, and the external structure after a Eurasian shield earth structure. The source is on the horizontal axis at the right edge of the plot. The amplitude is increased in a band above and to the left of the inclusion in both cases, and decreased above that. However, there are some interference effects in the finite difference calculation that are not reproduced in the Born calculation.**

Tectonic release could cause the observed ~factor of 2 offset between the two station sets. If, for example, tectonic release had the mechanism of a normal fault with tension in the east-west direction, it would amplify stations to the west more than to the north. However, to cause a factor of 2 difference would require a secondary source large enough that large Love waves would also be expected. No Love waves are apparent in any of the data. In any case, path structure seems a more likely cause of the variability, and it is possible that the variations would be predictable with higher resolution earth models, and/or a more accurate method for accounting for structural variations.

One final issue is the most appropriate measurement of  $M_s$  derived from spectra. In our previous work, and in the discussion above of the path corrected spectral magnitude, we have used a robust mean value as the best estimate. Bonner et al., 2006, however, have instead used the maximum value of the Butterworth filtered  $M_s$ . This has some advantage in discrimination, because although the corrections flatten explosion spectra, they do not quite flatten earthquake spectra, which tend to be larger at lower frequencies. So in principle the  $M_s$  value for explosions is frequency independent, while the earthquake  $M_s$  can choose a higher value, improving the  $M_s$ :mb discriminant. As the explosion spectra above demonstrate, however, there are variations in the explosion spectra also, and choosing the maximum point can lead to an  $M_s$  that is too high, degrading discrimination. We made one modification to Bonner et al.'s  $M_s$ (VMAX) procedure by implementing a simple outlier rejection test—we calculate the mean and standard deviation of the magnitudes and reject outliers greater than two standard deviations from the mean. We

then recalculate the mean and repeat the outlier rejection, using the remaining points to calculate either the mean or maximum magnitude. Table 2 shows a comparison of magnitudes for this event using the different methods. The results show that the mean value estimates are more consistent than the peak value estimates.

**Table 2. Station and network mean values for Ms as calculated using the methods described in the text.**

Station	Distance (km)	Ms(b) Mean	Ms(b) Peak	Ms(bp) Mean	Ms(bp) Peak	Ms(sp) Mean
MDJ	369	2.65	2.71	2.67	2.73	2.69
KSRS	440	2.69	2.75	2.70	2.74	2.76
INCN	476	2.68	2.80	2.69	2.78	2.81
BJT	1103	3.03	3.18	3.02	3.13	3.07
HIA	1148	2.93	3.07	2.93	3.08	3.00
ENH	2147	3.01	3.21	3.06	3.23	3.20
TLY	2252	3.00	3.25	3.09	3.32	3.16
<b>Mean (SD)</b>		2.86 (0.18)	3.00 (0.23)	2.88 (0.19)	3.00 (0.25)	2.96 (0.20)

### CONCLUSIONS AND RECOMMENDATIONS

We are attempting to understand and model the generation and propagation of surface waves in the 8–15 second period band in Eurasia. We model source excitation, receiver amplification and path dispersion and attenuation using earth models derived from a large global dispersion data set and relatively generic attenuation models. We then examine the residual and try to separate remaining path attenuation and variations due to path structure. We model the effect of heterogeneous structure using the Born approximation; however, the structural complexity and high frequencies required appear to push the Born approximation beyond its limits. We develop a path corrected surface wave magnitude which combines the time domain narrow-band surface wave magnitude procedure of Russell (2006) with the path corrected spectral magnitude of Stevens and McLaughlin (2001). We find that the Russell magnitude is a good match to the average value of the path corrected magnitude; however, there are substantial path and site specific variations that can be accounted for with the path corrected magnitude.

### REFERENCES

- Bonner, J. L., D. R. Russell, D. G. Harkrider, D. T. Reiter, and R. B. Herrmann (2006). Development of a time-domain, variable period surface-wave magnitude measurement procedure for application at regional and teleseismic distances—Part II: Application and  $M_s$ - $m_b$  performance, *Bull. Seism. Soc. Am.*, 96: 678–696, doi: 10.1785/0120050056.
- Rezapour, M. and R. G. Pearce (1998). Bias in surface-wave magnitude  $M_s$  due to inadequate distance corrections,” *Bull. Seism. Soc. Am.* 88: 43–61.
- Russell, D. R. (2006). Development of a time-domain, variable period surface-wave magnitude measurement procedure for application at regional and teleseismic distances—Part I: Theory, *Bull. Seism. Soc. Am.* 96: 665–677, doi: 10.1785/0120050055.
- Stevens, J. L. and K. L. McLaughlin (2001). Optimization of surface wave identification and measurement, *Pure Appl. Geophys.* 158: 1,547–1,582.
- Stevens, Jeffrey L., Jeffrey W. Given, G. Eli Baker, and Heming Xu (2006). Development of surface wave dispersion and attenuation maps and improved methods for measuring surface waves, in *Proceedings of the 28<sup>th</sup> Annual Seismic Research Review: Ground-Based Nuclear Explosion Monitoring Technologies*, LA-UR-06-5471, Vol. 1, pp. 273–282.
- Stevens, J. L., D. A. Adams, G. E. Baker, M. G. Eneva, and H. Xu (2005). Improved surface wave dispersion models, amplitude measurements and azimuth estimates, SAIC final report submitted to AFRL under contract DTRA01-01-C-0082, March.
- von Seggern, D. H. (1977). Amplitude-distance relation for 20-second Rayleigh waves, *Bull. Seism. Soc. Am.* 67: 405–411.
- Zhou, Y., F. A. Dahlen and G. Nolet (2004), Three-dimensional sensitivity kernels for surface wave observables, *Geophys. J. Int.* 158: 142–168.